Bohai sea front detection using BJ-1 small satellite data

PING Bo[1], SU Fenzhen[2], DU Yunyan[2], SU Weiguang[3]

1. *School of Remote Sensing and Information Engineering, Wuhan University, Wuhan* 430079, *China*;
2. *State Key luboratory of Recources and Environmental Information system, Institute of Geographic Sciences and Natural Resources Research, CAS, Beijing* 100101, *China*;
3. *Key Laboratory of Coastal Zone Environmental Processes, Yantai Institute of Coastal Zone Research, CAS, Yantai Shandong* 264003, *China*

Abstract: Fronts in the Bohai sea are detected based on BJ-1 small satellite data using a gravitation model.We select the red band as the experimental band due to the characters of small satellite data. In addition, the fronts south of the Bohai Bay and east of the Liaodong Bay are chosen as experimental areas because they are both eligible for front detection. In the experiments, a linear stretch and band computation are first applied to data in order to protrude front information. The stretch intervals are set according to histograms. Then, utilizing a gravitation model, the fronts can be extracted from preprocessed data,and the results show that fronts can be successfully extracted from BJ-1 small satellite data usingthe gravitation model. The detected fronts are continuous and obvious. Compared with traditional front detection algorithms, the proposed algorithm can not only detect continuous and conspicuous fronts, but can also suppress noises.

Key words: BJ-1 small satellite, model of universal gravity, front detection, Bohai sea

CLC number: P71 **Document code**: A

Citation format: **Ping B, Su F Z, Du Y Y and Su W G. 2014. Bohai sea front detection using BJ-1 small satellite data. Journal of Remote Sensing, 18(3): 000-000 [DOI: 10.11834/jrs.20143221]**

1 INTRODUCTION

Fronts are narrow boundaries existing between two or more water masses that have characteristics that are clearly different. Fronts can be depicted by a horizontal gradient or higher order derivatives of temperature, salinity, density, velocity, color, chlorophyll, and so on. In other words,a front can be detected based on one or more of the characteristics mentioned above (Li & Su, 2000; Su, et al., 2005). In recent times, there have been very few of these studies. In addition, front detection in the Bohai Sea is based mainlyon image interpretation or other methods that can be used for traditional satellite data such as Landsat, SPOT, and so on. Due to limitations faced by traditional satellites such as image quality, temporal resolution, data price, andso forth, front detection in the Bohai Sea is limited.

With the rapid development of small satellites, small-satellite technology has developed from an exploration period to a scientific application period. Also, small satellites have become a significant part of the satellite industry, and have significantly complemented traditional satellites (Ji, 2009; Wang, 2002). Due to the characteristics of small satellites, studies involving small satellites have always highlighted scientific studies.In particular, the development of small-satellite asterisms and constellation will replace some functions of many modern and large application satellites, and this kind of replacement has led to significant revolutions in satellite applications and the development of space technology (Xie& Wei, 2000). BJ-1 small satellite (BJ-1), which is a high-powered earth observation small satellite, can provide timely, reliable, and quality data services for city planning, ecological environment monitoring, major engineering monitoring, and land use monitoring,etc.However, ocean monitoring, particularly front detection, has still not been fully developed based on small satellites. Hence based on the characteristics of small satellites, studies on front detection algorithms for small satellite data are important.

Sun, et al., (2007) proposed an edge algorithm based on the gravitational method. In his algorithm, every pixel in each image is regarded as an object, and its pixel value is regarded as its mass. Every pixel and its 3 × 3 neighboring pixels can form a subarea. According to the law of gravity, in each subarea, we can calculate the gravitational forces that act on the central pixel due to neighboring pixels. Based on the Ostu algorithm, a threshold can be set and an edge image can be acquired by comparing every pixel's force and threshold. Zhang & Chen(2011) replaced the quality of the central pixel in each subarea with a function, where two nonlinear gradients are regarded as variables, and they

Received: 2013-08-14; **Accepted**: 2013-12-12; **Version of record first published**: 2013-12-19
Foundation: National Key Technology R&D Program of China (No.2011BAH23B04)
First author biography: PING Bo (1986—), male, Ph.D. candidate. He majors in oceanography in remote sensing. E-mail: pingb@lreis.ac.cn
Corresponding author biography: SU Fenzhen (1972—), male researcher. His current research interests include GIS for oceanography based on spatial and temporal sequence. E-mail: sufz@lreis.ac.cn

also used Sun's algorithm to extract edges. Lopez-Molina (2010) analyzed the influences from neighborhood selection, gravitational formula transformations, etc. in Sun's algorithm. Ping et al., (2013) proposed a gravitational model based on Sun's algorithm, and utilized the model to detect a part of the Kuroshio front. In addition, there sults in Ping's paper can prove the effectiveness and superiority of the gravitational model in front detection. However, front detection based on small-satellite multi-spectral data obtained by using a gravitational model has not been fully developed, and more focus is required in this field.

Hence, based onthe analyses mentioned above, this paper presents some front detection results obtained in the Bohai sea based on BJ-1 data. The main research areas in this paper are south of the Bohai Bay and east of Liaodong Bay.

2 SMALL-SATELLITE DATA ANALYSIS

2.1 Analysis of BJ-1 data

As a member of the international disaster monitoring constellation, BJ-1's multi-spectral sensor is composed of two linear push-broom CCD imagers, and each imager contains a near-infrared band, a red band, and a green band. In practice, two imagers work simultaneously. The number of CCD photosensitive images acquired from each camera for each band is 9984, so the number of CCD photosensitive images acquired from the two cameras is 19400 (including 560 overlapped CCD photosensitive images). The spatial revolution of the multi-spectral data of the BJ-1 is 32 m, and the image's multi-spectral data spans a 600 km area. This large image coverage can substantially shorten the satellite orbital period, and is therefore promising for large-scale oceanic monitoring. Multi-spectral data with a spatial revolution of 32 m can be acquired within two days. The scroll angle of the satellite is 0.02° and the area spanned by each imageis 458.656 × 319.488 km ((14333 × 32 = 458656 m)× (9984 × 32 =319488 m)).The main specifications of the BJ-1 are shown in Table 1. BJ-1 carries a wide-view imager with a spatial revolution of 32 m, and its bands correspond to band 2, band 3, and band 4 of Landsat TM. The specific bands ranges of BJ-1 are shown in Table 2.

Table 1 Main specifications of BJ-1 satellite

Name	Specifications
Orbit	Three axis stabilized sun synchronous orbit
Orbit height/km	686
Orbit inclination angle/(°)	98.1725
Imaging mode	Ascending node imaging, local time 10:30—11:30
Useful load	Multi-spectral sensor Panchromatic sensor
Data transportation	Xband:40/20 Mbps Sband:8 Mbps
Satellite storage capacity	240 G hard disk+4 G solid state memory

Table 2 Comparison between BJ-1 and Landsat TM

Satellite	Spectral range/μm		
	Green	Red	Near-infrared
BJ-1	0.523—0.605	0.630—0.690	0.774—0.900
Landsat TM	0.520—0.600	0.630—0.690	0.760—0.900

2.2 Analysis of BJ-1 data in the Bohai sea

In this paper, the areas south of the Bohai Bay and east of Liaodong Bay were selected as the experimental areas. The Bohai Bay area was obtained from multi-spectral small satellite data acquired on October 14,2007,and that of the Liaodong Bay area was obtained from data acquired on April 26,2009. The specific data are shown in Fig.1 and Fig.2, respectively. To the south of the Bohai Bay, due to different silt contents, an obvious front can be seen in the small satellite image; similarly, the radial sand ridge in the Liaodong Bay is also conspicuous in small satellite images.

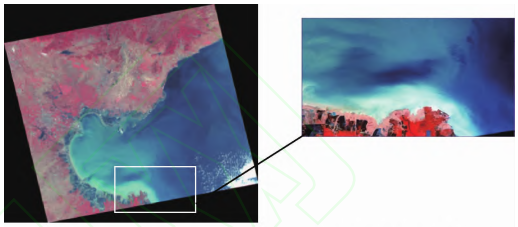

(a) Bohai Bay (b) Experimental area

Fig.1 Bohai Bay imaged on October 14, 2007

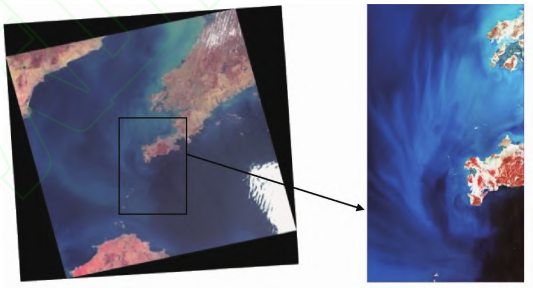

(a) Liaodong Bay (b) Experimental area

Fig.2 Liaodong Bay imaged on April 26, 2009

In summary, some main characters of BJ-1 small-satellite data in the Bohai Sea are:

(1) There is an obvious front to the south of the Bohai Bay. From thearea selected by the rectangle frame, we see that the shape of the front in this area is mainly arched. In the near shore area,there is higher silt content relative to the peripheral sea; hence, a conspicuous boundary can be seen in Fig.1 and the boundary needs to be extracted. We can obtain this front by using visual interpretation based on image color.

(2) There is also an obvious front in the Liaodong Bay, and its shape is radial. In addition, the texture of this front is clear.

3 FRONT DETECTION BASEDON BJ-1DATA

3.1 Data processing

Because of the correspondence between BJ-1 multi-spectral data and band 2, band 3, and band 4 of the Landsat TM data, in order to select a suitable band for front detection, we first need to analyze the characteristics of the Landsat TM data. The second Landsat TM data band is green, and is sensitive to healthy and flourishing plants, and can be used to explore the reflection of plants. Based on the reflection of the green band, the condition

of plants can be evaluated, different forests can be distinguished, and underwater characteristics can be reflected; band 3 of the Landsat TM data is the red band, which is the main absorption band of chlorophyll. This band is widely used in the detection of the lay of the land, lithology, soil, plants, silt, and so on; band 4 of the Landsat TM data is the near-infrared band,which is sensitive to green plants and can be used for plant surveys, water area measurements, crop condition measurements, water area identification, and so on. Based on the analyses mentioned above, we select the red band of small-satellite data as the experimental band.

The experiment areasare show in Fig.3. Fig.4 shows the histograms of the red band forthe two experimental areas. We can see that in these two areas, the small-satellite data are very concentrated (the pixel values to the south of the Bohai Bay range from 0 to 96, and the pixel values to the east of Liaodong Bay range from 14 to 103), so the widths of the red band are narrow. Hence, the contrast ratios of the two sets of experimental data are low. Based on the above analyses, the data is processed to make the fronts prominent as well as suppress non-front information.

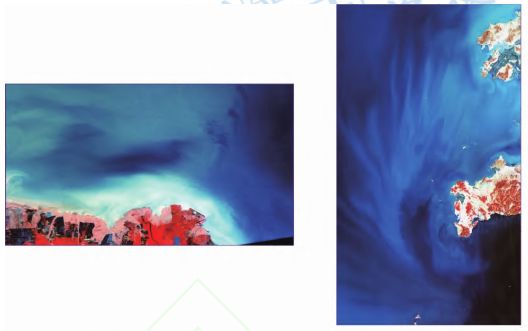

(a) South of Bohai Bay (b) East of Liaodong Bay

Fig.3 Experimental areas

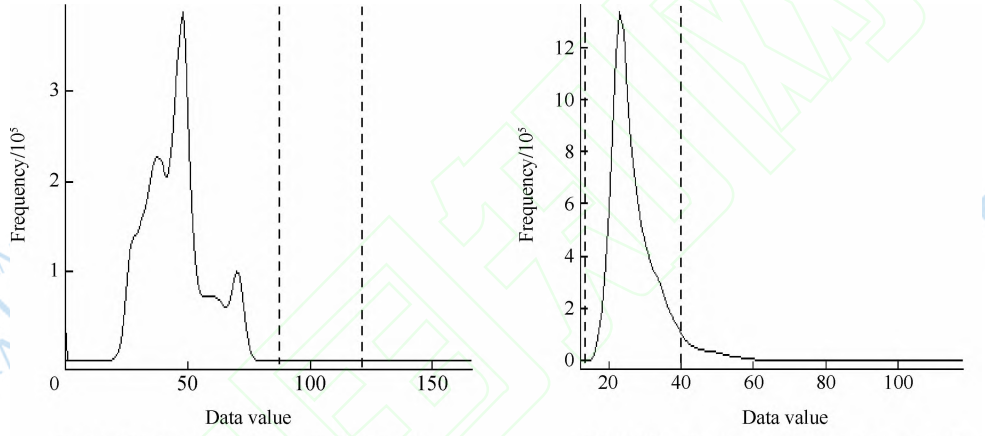

(a) Red band histogram for south of Bohai Bay (b) Red band histogram for east of Liaodong Bay

Fig.4 Red band histograms for regions south of the Bohai Bay and east of Liaodong Bay

Through careful analyses on the small-satellite data, we can see that most of the pixels in each image are non-front data, and so the peak of the histogram corresponds to these pixels; in addition, fronts and boundaries between the land and sea contain edge information. These edges contain a great deal of information and the values of these pixels are high, so these pixels may form the second peak after the first peak in the histogram. In order to enhance the contrast ratio and suppress noise, Eq.(1) is applied for band calculation.

$$new\_pixel(i,j) = \begin{cases} Max\_pixel - (B2(i,j) - B1(i,j)), B2(i,j) \geqslant B1(i,j) \\ B1(i,j), B2(i,j) < B1(i,j) \end{cases} \quad (1)$$

where $new\_pixel(i,j)$ is the result after band calculation, Max_pixel is the maximum data value in the original image, $B2(i,j)$ is the image after local stretch, $B1(i,j)$ is the original image. The intervals for the stretch areset based on histograms. After several experiments, we can see that when the stretch interval is set using low-value pixels, the result will contain much noise; when the stretch interval is set using high-value pixels, the result will suppress noises, but some front information will be overlooked. Hence, from the original images, we can see that the front to the south of the Bohai Bay is obvious, but non-front information has a serious effect on this area, so the stretch interval will be set by using high-value pixels. Similarly, the front to the east of Liaodong Bay is weak, so the stretch interval will be set using low-value pixels. The specific stretch intervals for the two images are shown in Fig.4 using white lines. Fig.5 shows results after data processing. From Fig.5, we can see that fronts are prominent and conspicuous after data processing. The gravitational model for front detection is applied to these preprocessed images,and the fronts can be extracted.

(a) South of Bohai Bay after data processing (b) East of Liaodong Bay after data processing

Fig.5 South of Bohai Bay and east of Liaodong Bay after data processing

3.2 Gravitational model

Front detection is easily affected by noises, and image noises will generate some useless results. The median filter is a highly efficient digital filtering technique that removes isolated noise while preserving the edges in the data (Belkin & O'Reilly, 2009). Hence, the median filter is applied toall of the images to remove some noises and tiny edges.

For pixels whose values are equal to 0, i.e., their masses are equal to 0, based on the gravitational method; we know that regardless of the values of pixels surrounding these pixels in their 3 × 3 neighborhood, the gravitational forces on these pixels are non-existent.These pixels therefore have an adverse effect on front detection. Hence, according to Lopez-Molina, et al., (2010), we modified these zero-value pixels using Eq.(2).

$$q_{new} = q_{old} + \xi q \tag{2}$$

where q_{new} is the value after calculation, q_{old} is the value of the zero-value pixel, ξq is a tiny positive number, and in this paper, this positive number is equal to 0.001.

The gravitational algorithm introduced by Sun, et al., (2007) requiresoriginal data. For example, as shown in Fig.6, Fig.6(a) and Fig.6(b) are both edges, yet the gravitational forces on the central pixels in Fig.6(a) and Fig.6(b) are different, and the force in Fig.6(b) is almost 10 times larger than that in Fig.6(a). Hence, it is possible to regard image Fig.6(a) as a non-front area by using a single threshold. Based on the above analysis, we normalize each 3 × 3 neighborhood using Eq.(3).

$$X_{new} = \frac{X_{old}}{max} \tag{3}$$

where X_{new} is the value after normalization, X_{old} is the value of the original pixel, and max is the maximum value in each 3 × 3 neighborhood.

2	3	2
2	3	2
20	30	20

(a) Small gravitation data

20	30	20
20	30	20
200	300	200

(b) Large gravitation data

Fig.6 An edge example

For each normalized 3 × 3 neighborhood, non-linear transformation is applied by using Eq.(4) to enhance the data contrast ratio.

$$X_{new}(i,j) = \begin{cases} 2X_{old}^2(i,j) & 0 \leqslant X_{old}(i,j) \leqslant 0.5 \\ 1 - 2(1 - X_{old}(i,j))^2 & 0.5 \leqslant X_{old}(i,j) \leqslant 1 \end{cases} \tag{4}$$

where $X_{new}(i,j)$ is the enhanced value of the pixel and $X_{old}(i,j)$ is the value of the normalized pixel.

Gravitational forces can be calculated for enhanced data by using the gravitational method introduced by Sun, et al., (2007). Then, a threshold is set and the final fronts can be acquired.

4 EXPERIMENTALRESULTSANDANALYSIS

4.1 Front detection results based on small-satellite data obtained using gravitational model

Front detection results for the area south of the Bohai Bay and east of the Liaodong Bay are shown in Fig.7. As shown in Fig. 7, the algorithm proposed in this paper can extract continuous front contours in both areas. Positioning accuraciesare rather high and noises in images are suppressed. In Fig.7(a), the white arrow indicatesthe extracted front. From the original data for the area south of the Bohai Bay, we observe that this front is a near-shore front. Compared with the boundary between the land and sea, this front is weak and is easily affected by noises and the boundary between land and sea. Using the proposed algorithm, this front is precisely distinguished, and this result is almost identical to the result obtained from visual interpretation. In Fig.7(b), although the area indicated by the white arrow is affected by noises, the entire shape of the radial sand ridge is extracted, and each branch of the radial sand ridge is continuous and sealed. Hence, from the above analyses, the proposed algorithm is suitable for front detection based on small-satellite data.

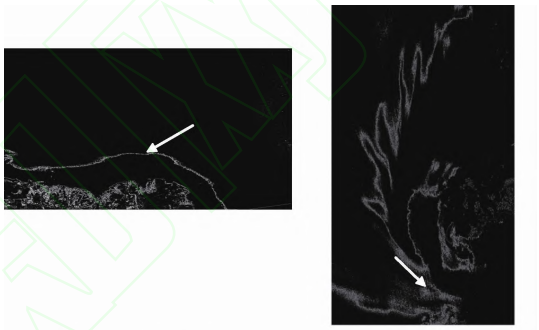

(a) Result forBohai Bay (b) Result for Liaodong Bay

Fig.7 Results for the Bohai area obtained using BJ-1 data

4.2 Front detection results based on different algorithms

Fig.8 shows front detection results for the south of Bohai Bay obtained using different algorithms. This front is nearshore, so on the one hand, compared with the boundary between the land and sea, the strength of this front is weak, and the front is easily affected by noises; on the other hand, compared with peripheral sea water, the nearshore area contains more silt, so the strength of this front is strong.Hence, the positioning accuracy is affected by nearshore silt. As shown in Fig.8, these three algorithms can all detect front contours, yet the Sobel algorithm and morphology algorithm are not as good as the proposed algorithm. As shown in Fig.8(a) and Fig.8(b), the positioning accuracies of the Sobelalgorithm andmorphology algorithm are low. In addition, the extracted fronts in Fig.8(a) and Fig.8(b) are not single lines. White arrows indicate thenearshore silt, and we can see that by using these two algorithms, nearshore silt has an adverse effect on the final results. Furthermore, the boundary between the land and sea is not clear in each final image. Due to normalization and enhancement processing in the proposed algorithm, the contrast ratio in the front area is boosted, and influences from non-front information are suppressed. As shown in Fig.8(c), the front extracted using theproposed algorithm is continuous, and the algorithm removes the influences caused by nearshore silt. In addition, the positioning accuracy is high and the shape of the front is identical with that of the visual interpre-

tation. Hence, the proposed algorithm is suitable for front detection based on small satellite data.

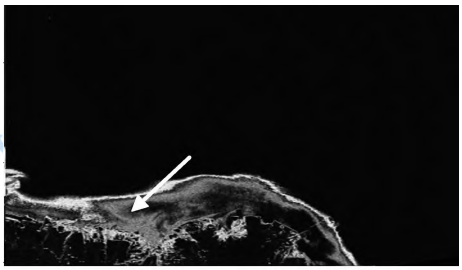

(a) Result of Sobel algorithm

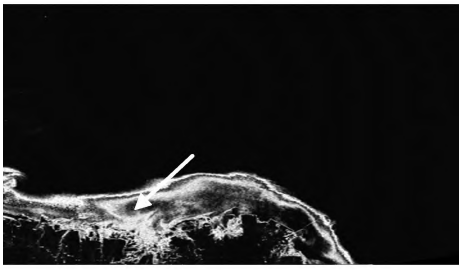

(b) Result of morphology algorithm

(c) Result of the proposed algorithm

Fig.8 Results of BJ-1 small-satellite data based on different algorithms

5 CONCLUSION

BJ-1 data are widely used in land use monitoring, city planning, and so on, but there are few applications regarding front detection based on small-satellite data. Front detection in the Bohaisearelies mainly on traditional visual interpretation, and automatic front detection based on satellite data thereforerequires more study. Hence, in this paper, an algorithm is developed and is used for BJ-1 data.

In this paper,a gravitational model is applied to front detection in the Bohai Sea. According to the characteristics of the BJ-1 data, the red band is selected as an experimental band, and because of large quantities ofdata, a stretch algorithm was proposed. After stretch and band calculation, the gravitational model is applied for front detection. From our results, we can see that the proposed algorithm is suitable for small-satellite data to detect fronts in the Bohai Sea. In addition, the fronts detected are continuous and complete. Compared with traditional front-detection algorithms, the proposed algorithm can obtain better results.

REFERENCES

Belkin I M and O'Reilly J E. 2009. An algorithm for oceanic front detection in chlorophyll and SST satellite imagery. Journal of Marine Systems, 78(3): 319-326 [DOI: 10.1016/j.jmarsys.2008.11.018]

Ji K. 2009. The image analysis of the "Beijing-1" small satellite. Spacecraft Recovery & Remote Sensing, 30(1): 38-42

Li F Q and Su Y S. 2000. Water Masses Analysis. Qingdao: China Ocean University Press: 29-36

Lopez-Molina C, Bustince H, Fernandez J, Couto P and De Baets B. 2010. A gravitational approach to edge detection based on triangular norms. Pattern Recognition, 43(11): 3730-3741 [DOI: 10.1016/j.patcog.2010.05.035]

Ping B, Su F Z, Du Y Y, Meng Y S and Su W G. 2013. Application of the model of universal gravity to oceanic front detection near the Kuroshio front. Journal of Geo-information Science, 15(2): 187-192

Su F Z, Zhou C H, Yang X M, Zhang J and Luo J C. 2005. Marine Geographic Information System: Principle, Technique, Application. Beijing: China Ocean Press: 39

Sun G Y, Liu Q H, Liu Q, Ji C Y and Li X W. 2007. A novel approach for edge detection based on the theory of universal gravity. Pattern Recognition, 40(10): 2766-2775

Sun Y T. 1999. The technique of small satellite. Telecommunication Information, (4): 13-15

Wang X H. 2002. The development of small satellite. Aerospace China, (1): 9-14

Xie W J, Wei Y C, Ni S X and Zuo W. 2000. The progress of small satellite. Remote Sensing Information, (3): 41-44

Zhang C X and Chen X H. 2011. Gravitational approach to edge detection based on nonlinear filtering. Journal of Computer Application, 31(3): 763-766

北京一号数据检测渤海海洋锋

平博[1]，苏奋振[2]，杜云艳[2]，苏伟光[3]

1.武汉大学遥感信息工程学院，武汉 430079；
2.中国科学院地理科学与资源研究所资源与环境信息系统国家重点实验室，北京 100101；
3.中国科学院海岸带环境过程重点实验室(烟台海岸带研究所)，烟台 264003

摘　要：本文基于引力模型，对北京一号对地观测小卫星数据渤海区域进行海洋锋面检测。针对北京一号小卫星数据的特点，选择红波段作为实验波段，并选择渤海湾南岸水色锋和辽东湾东岸辐射沙脊两个实验区域。算法首先对数据进行线性拉伸，波段运算等预处理，突出锋面信息，其中，拉伸区间由图像直方图确定，接着应用引力模型对预处理后的数据进行锋面检测。实验结果表明，本文算法能够对两个实验区域的锋面进行检测，得到的锋面信息连续、突出，证明了算法的有效性；针对北京一号对地观测小卫星数据，本文算法相比于传统锋面检测算法，能够得到更加连续的锋面信息，并能较好抑制近岸泥沙对锋面检测的干扰。

关键词：北京一号小卫星，引力模型，锋面提取，渤海

中图分类号：P71　　**文献标志码**：A

引用格式：平博，苏奋振，杜云艳，苏伟光. 2014. 北京一号数据检测渤海海洋锋. 遥感学报，18(3)：000-000

Ping B, Su F Z, Du Y Y and Su W G. 2014. Bohai sea front detection using BJ-1 small satellite data. Journal of Remote Sensing, 18(3): 000-000 [DOI: 10.11834/jrs.20143221]

1　引　言

海洋锋指特性明显不同的两种或几种水体之间的狭窄过渡带。它们可用温度、盐度、密度、速度、颜色、叶绿素等要素的水平梯度，或它们的更高阶微商来描述；即一个锋带的位置可以用一个或几个上述要素特征量的强度来确定(李凤岐和苏育嵩，2000；苏奋振 等，2005)。目前，渤海区域的锋面研究较少，且该区域的锋面提取多是基于目视解译，或是基于 Landsat、SPOT 等大卫星数据进行锋面的检测，因大卫星数据受成像质量、运行周期、价格等限制，其锋面检测，尤其是渤海区锋面检测的实用性受到限制。

经过几十年快速发展，小卫星技术已经从探索研究阶段发展到科学应用阶段，成为卫星家族不可缺少的重要一员，也是大卫星的必要补充(纪凯，2009；王晓海，2002)。小卫星以其“快、好、省”的特点，一直是科学研究的重点(纪凯，2009；孙宇彤，1999)。特别是小卫星星群或星座的发展，将取代部分现代大型应用卫星的功能，已经引起卫星应用和空间技术发展的重大变革(谢文君 等，2000)。北京一号对地观测小卫星(北京一号)是高性能对地观测小卫星，可以为城市规划、生态环境监测、重大工程监测和土地利用监测等提供及时、可靠和优质的数据服务，但目前应用小卫星数据进行海洋监测，特别是海洋锋的检测研究仍然较少。针对小卫星的成像和数据特点，研究基于小卫星数据的锋面检测算法势在必行。

Sun 等(2007)提出使用万有引力算法进行边缘的检测，其是将数字影像的每一个像素点都作为一个天体，并将其像素值作为其质量，根据牛顿的万有引力定律，计算邻域像素对中心点的引力和，得到引力幅值，并基于 Ostu 方法得到阈值，最终得到边缘影像。张春雪和陈秀宏(2011)利用两个非线性梯度为自变量的函数代替中心像素点的质量，并结合万有引力算法进行边缘检测。Lopez-Molina 等

收稿日期：2013-08-14；**修订日期**：2013-12-12；**优先数字出版日期**：2013-12-19
基金项目：国家科技支撑项目(编号：2011BAH23B04)
第一作者简介：平博(1986—)，男，博士研究生，主要从事海洋遥感研究。E-mail:pingb@lreis.ac.cn
通信作者简介：苏奋振(1972—)，男，研究员，主要从事时空序列海洋地理信息系统研究。E-mail:sufz@lreis.ac.cn

(2010)对万有引力算法进行了分析，讨论了邻域选取、引力公式变体等因素对该算法的影响。平博等(2013)提出基于万有引力算法的引力模型，并应用该模型利用海洋表面温度数据，对黑潮锋面进行了检测，证实了引力模型的有效性和在锋面检测方面的优越性。但基于引力模型对小卫星多光谱数据进行海洋锋检测的应用还比较少，有待基于小卫星数据对该模型进行进一步的实验分析。

因此，本文采用北京一号数据，基于引力模型进行渤海区域海洋锋面的检测。主要的研究区域是渤海湾南岸区域的水色锋检测和辽东湾东岸区域的辐射沙脊检测。

2 北京一号数据分析

2.1 北京一号数据分析

作为国际灾难监测星座的一员，北京一号多光谱遥感器由两组线性 CCD 推扫式成像仪构成，每一组成像仪由近红外波段、红波段和绿波段组成。在实际成像过程中，双成像仪同时成像，每一波段相机的 9984 个 CCD 感光成像，同一波段的两个相机共获取 19400 个 CCD 成像的地面幅宽(包含左右相机 560 个 CCD 的成像重叠)。小卫星的多光谱相机分辨率为 32 m，多光谱图像的图像幅宽达到 600 km，这样的大幅宽缩短了图像重访周期，更加有利于对海面进行大尺度的实时监测，32 m 多光谱数据在 2 天内可以获取。小卫星成像时卫星侧摆角为 0.02°，单景影像覆盖面积长为 14333×32=458656 m，即 458.656 km，宽为 9984×32=319488 m，即 319.488 km。北京一号的主要技术指标如表 1 所示。北京一号上搭载的 32 m 宽视场成像仪，对应着 Landsat TM 的波段 2、波段 3、波段 4，但也有细微差别，具体如表 2 所示。

表 1 北京一号小卫星主要指标

指标名称	具体指标
轨道	三轴稳定太阳同步轨道
轨道高度/km	686
轨道倾角/(°)	98.1725
成像方式	升交点成像，地方时 10:30—11:30
有效载荷	多光谱传感器 全色传感器
数据传输	Xband:40/20 Mbps Sband:8 Mbps
星上存储容量	240 G 硬盘+4 G 固态存储器

表 2 小卫星数据和 TM 数据比较

卫星	光谱范围/μm		
	绿	红	近红外
北京一号	0.523—0.605	0.630—0.690	0.774—0.900
Landsat TM	0.520—0.600	0.630—0.690	0.760—0.900

2.2 北京一号渤海区域数据分析

本文选择渤海湾南岸和辽东湾东岸两个区域作为研究区，其中，渤海湾数据为 2007 年 10 月 14 日的北京一号多光谱数据，辽东湾数据为 2009 年 4 月 26 日的北京一号多光谱数据，具体数据如图 1 和图 2 所示。在渤海湾南岸，由于泥沙含量的不同，能够在北京一号数据上形成明显水色锋；辽东湾东部的辐射沙脊也能够在北京一号数据上得到显示。

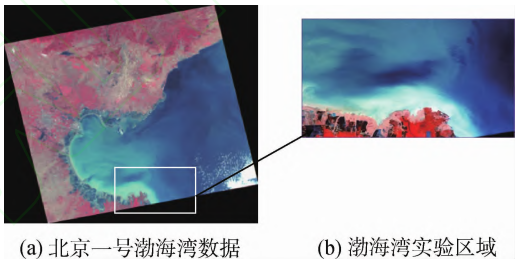

(a) 北京一号渤海湾数据 (b) 渤海湾实验区域

图 1 2007 年 10 月 14 日渤海湾

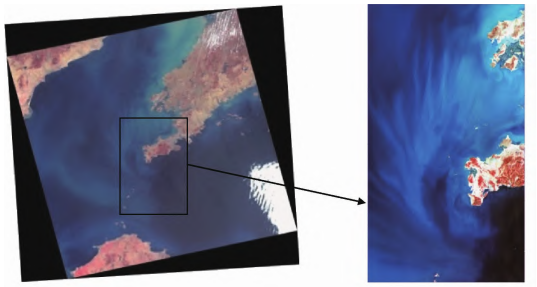

(a) 北京一号辽东湾数据 (b) 辽东湾实验区域

图 2 2009 年 4 月 26 日辽东湾

总体而言，北京一号数据在渤海区域的特点主要有：

(1)渤海湾南岸海洋锋明显，从图 1 中框选区域可以看出，渤海湾南岸水色锋多呈弧线状，泥沙含量高的近岸区域海水色度较亮，与泥沙含量低的外围海水有明显的分界，可以从图像色度上进行目视解译。

(2)辽东湾东部地区的辐射沙脊在小卫星图像上成像明显，呈向外辐射状，纹理清晰。

3 北京一号海洋锋检测

3.1 北京一号数据处理

因为北京一号多光谱数据与 Landsat TM 数据波段 2、3、4 相近,因此,对 Landsat TM 数据波段 2、3、4 进行分析,选择合适波段进行渤海海洋锋检测。Landsat TM 数据波段 2,即绿波段,对健康茂盛植物的反射敏感,用于探测健康植物绿色反射率,按绿峰反射评价植物的生活状况,区分林型,树种和反映水下特征;Landsat TM 数据波段 3,即红波段,该波段为叶绿素的主要吸收波段,广泛用于地貌,岩性,土壤,植被,水中泥沙等方面的检测;Landsat TM 数据波段 4,即近红外波段,对绿色植物类别差异最敏感,用于目视调查,作物长势测量,水域测量,生物量测定及水域判别。通过以上分析,本文选择北京一号小卫星多光谱数据红波段作为实验波段。

图 3 为本文的实验区域。从图 4 所示的两个实验区域的红波段直方图可以看出,小卫星该波段数据较为集中(渤海湾南岸实验数据灰度分布在 0—96 之间;辽东湾东岸实验数据灰度分布在 14—103 之间),波段宽度较窄,其数据对比度较低,锋面检测能力较低。因此需要对数据进行预处理,突出锋面信息,并抑制非锋面信息。

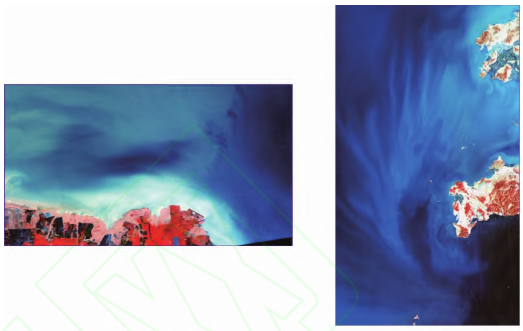

(a) 渤海湾南岸区域 (b) 辽东湾东岸区域

图 3 实验区域

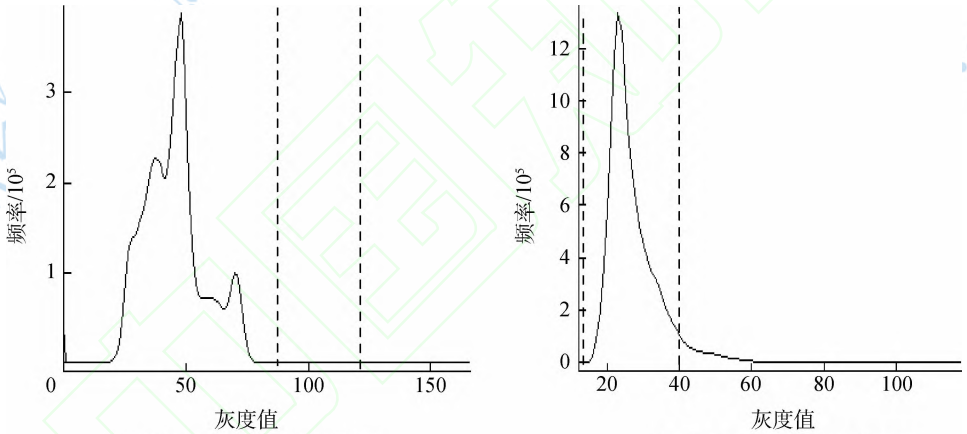

(a) 渤海湾南岸红波段直方图 (b) 辽东湾东岸红波段直方图

图 4 渤海湾和辽东湾北京一号数据红波段直方图

分析小卫星数据可以发现,海面非锋面区域的数据占图像的大部分像素,所以,最高的波峰应该对应该类像素,而锋面和海陆边缘是边缘信息,同样包含大量信息,而且锋面像素的值在整幅图像中偏大,因此,该类像素形成最高波峰后的第 2 个波峰。为了增大锋面的对比度并滤除噪声的干扰,采用式(1)对原始图像进行波段运算处理。

$$new\_pixel(i,j)=\begin{cases}Max\_pixel-(B2(i,j)-B1(i,j)), & B2(i,j)\geqslant B1(i,j)\\ B1(i,j), & B2(i,j)<B1(i,j)\end{cases} \tag{1}$$

式中,$new\_pixel(i,j)$ 为预处理后数据,Max_pixel 为图像中的最大像素值,$B2(i,j)$ 为局部拉伸后图像,$B1(i,j)$ 为原始图像,其中 $B2(i,j)$ 图像的拉伸区间通过直方图确定。通过试验发现,当拉伸区间偏向低像素值时,其拉伸结果含有较多的噪声;当拉伸区间偏向高像素值时,其拉伸结果的噪声较少,但锋面信息损失较大。鉴于此,原始图像中,渤海湾南岸区域锋面信息较明显,但受到噪声的干扰较大,因此,拉伸区间偏向像素值较大区域;辽东湾东岸区域锋面信息较弱,因此,拉伸区间偏向低像素值区域。具体拉伸区间见图 4 中虚线区间所示。图 5 为预处理后结果,从图 5 可以看出,预处理后的图像锋面信息更加突出,噪声干扰较小。对预处理后的数据进行基于引力模型的海洋锋检测,得到渤海两个实验区域的锋面检测结果。

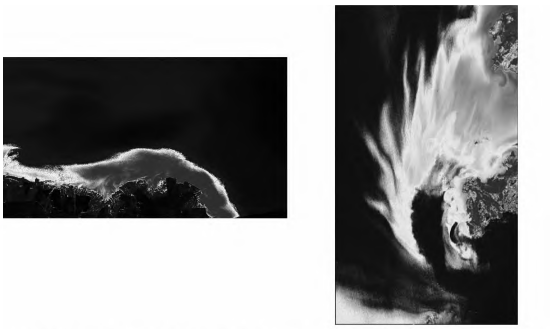

(a) 预处理后渤海湾南岸图像 (b) 预处理后辽东湾东岸图像

图 5 预处理后渤海湾南岸和辽东湾东岸图像

3.2 引力模型

海洋锋检测极易受到噪声的干扰，从而对最终的结果产生影响。中值滤波是一种高效的滤波技术，能够在滤除噪声的同时，保持边缘的细节(Belkin 和 O'Reilly, 2009)。对此，采用中值滤波算子遍历图像，滤除预处理后数据中的噪声和细小边缘。

对于数据中像素值为 0 的点，即质量为 0，基于引力公式可知，无论其邻域像素的值是多少，该像素的引力值都为 0，这样会对最后的锋面检测造成干扰。因此，基于 Lopez-Molina 等(2010) 中的介绍，利用式(2)对像素值为 0 的点进行修正。

$$q_{new} = q_{old} + \xi q \tag{2}$$

式中，q_{new} 为变换后的像素值，q_{old} 为像素值为 0 的点的像素值，ξq 为一个极小的正数，本文取 0.001。

Sun 等(2007)中提出的万有引力边缘检测算法依赖于原始数据的明暗程度，如图 6 所示，图 6(a)和图 6(b)都是两个边缘区域，但图 6(a)和图 6(b)区域对中心像元的引力相差 10 倍，因此基于单一阈值的锋面检测，可能将图 6(a)区域作为非锋面区域，从而造成锋面漏检。因此，针对每一个 3×3 的区域，均采用式(3)将其区域内的像元进行归一化。

$$X_{new} = \frac{X_{old}}{max} \tag{3}$$

式中，X_{new} 为归一化后像素值，X_{old} 为原始像素值，max 为 3×3 区域内的最大值。

2	3	2
2	3	2
20	30	20

(a) 小引力边缘模拟数据

20	30	20
20	30	20
200	300	200

(b) 大引力边缘模拟数据

图 6 边缘实例

针对归一化后的 3×3 邻域，采用式(4)进行非线性变换，增强数据对比度。

$$X_{new}(i,j) = \begin{cases} 2X_{old}^2(i,j) & 0 \leqslant X_{old}(i,j) \leqslant 0.5 \\ 1 - 2(1 - X_{old}(i,j))^2 & 0.5 \leqslant X_{old}(i,j) \leqslant 1 \end{cases} \tag{4}$$

式中，$X_{new}(i,j)$ 为增强后像素值，$X_{old}(i,j)$ 为原始像素值。

基于 Sun 等(2007)中的引力算法，对增强后的数据进行引力计算，继之，设定阈值，获得海洋锋信息。

4 实验结果与分析

4.1 基于引力模型的小卫星锋面检测结果

对渤海湾南岸和辽东湾东岸的水色锋和辐射沙脊进行锋面检测的结果如图 7 所示。从结果图中可以看出，本文算法对两个实验区域都能够提取出连续的锋面轮廓，提取的锋面定位精度高，并能较好的抑制噪声等的干扰。在 7(a)图中，箭头所示为提取的锋面，从图 1 的原始数据可以看出，该水色锋属于近岸锋面，相比海陆边缘，该锋面在图像上属于弱信息，极易受到噪声和海陆边缘的影响。但本文算法不仅能够很好的区分该锋面和海陆边缘，并且能准确定位近岸泥沙与外围海水差异最大的分界线，与目视解译的效果相当；在 7(b)图中，虽然在箭头所示的辐射沙脊的南岸部分会受到部分噪声的干扰，但沙脊的整体形状能够完整提取，并且提取的沙脊每一个分支都连续封闭。因此，从检测结果和以上分析可以看出，本文算法适合小卫星数据的锋面检测。

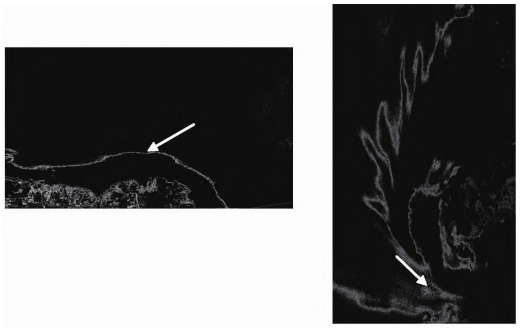

(a) 渤海湾南岸水色锋检测结果 (b) 辽东湾东岸辐射沙脊锋面检测结果

图 7 渤海北京一号锋面检测结果

4.2 基于不同算法的北京一号锋面检测结果

图 8 为基于不同算法对渤海湾南岸水色锋预处

理后数据的锋面检测结果。该水色锋属于近岸锋,相比海陆边缘,该锋面在图像上属于弱信息,极易受到噪声的干扰;另一方面,该区域的近岸泥沙相比外围海水在图上属于强信息,锋面定位精度较易受到近岸泥沙的干扰。从图 8 可以看出,3 种算法都能得到锋面的大致轮廓,但 Sobel 算法和形态学算法的检测结果并不理想。从图 8(a)和图 8(b)的检测结果可以看出,两种算法的锋面定位精度较低,得到的锋面不能呈单一的线状,图 8 中箭头所示区域为近岸泥沙,可以看出,这两种算法并没有去除近岸泥沙对锋面检测的影响,并且海陆边缘不够清晰,检测效果较差。本文提出的引力模型通过归一化和增强算法,增大锋面区域的对比度,同时,降低非锋面区域的干扰。从图 8(c)中可以看出,本文算法提取的锋面连续,而且消除了近岸泥沙对锋面检测的干扰,定位精度较高,锋面形状与目视解译相当,海陆边缘清晰。因此,本文算法适用于北京一号数据的海洋锋检测。

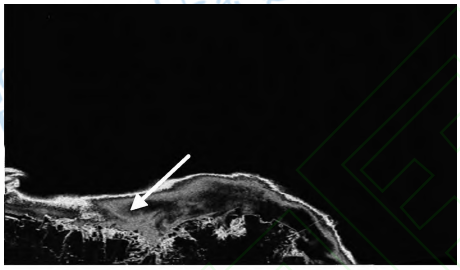

(a) Sobel算子检测结果

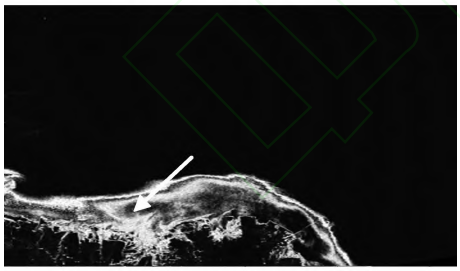

(b) 形态学梯度检测结果

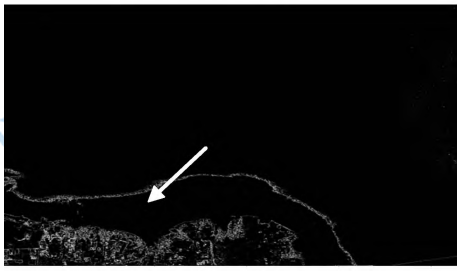

(c) 引力模型检测结果

图 8 基于不同算法的北京一号小卫星数据检测结果

5 结 论

北京一号小卫星数据广泛用于土地利用监测,城市规划等方面,但基于该数据进行锋面检测的应用仍不多。渤海区域的锋面检测多是基于传统目视解译,但基于卫星数据的自动锋面检测仍不多。因此,本文基于北京一号小卫星数据进行渤海区域的锋面检测。

本文应用引力模型对渤海区域进行锋面检测。根据小卫星数据的特点,选择红波段作为试验波段,并根据波段数据分布较集中的特点,对数据进行拉伸,波段运算等预处理,最后基于引力模型进行锋面检测。实验结果表明,本文算法能够对北京一号数据进行锋面检测,得到的锋面较连续,锋面对比度高;相比于传统锋面检测算法,本文算法更适合于小卫星数据的锋面检测。

参考文献(References)

Belkin I M and O'Reilly J E. 2009. An algorithm for oceanic front detection in chlorophyll and SST satellite imagery. Journal of Marine Systems, 78(3): 319-326 [DOI: 10.1016/j.jmarsys.2008.11.018]

纪凯. 2009. "北京一号"小卫星图像分析. 航天返回与遥感, 30(1): 38-42

李凤岐, 苏育嵩. 2000. 海洋水团分析. 青岛: 青岛海洋大学出版社: 29-36

Lopez-Molina C, Bustince H, Fernandez J, Couto P and De Baets B. 2010. A gravitational approach to edge detection based on triangular norms. Pattern Recognition, 43(11): 3730-3741 [DOI: 10.1016/j.patcog.2010.05.035]

平博, 苏奋振, 杜云艳, 孟云闪, 苏伟光. 2013. 基于引力模型的海洋锋信息提取. 地球信息科学, 15(2): 187-192

苏奋振, 周成虎, 杨晓梅, 张杰, 骆剑承. 2005. 海洋地理信息系统: 原理, 技术与应用. 北京: 海洋出版社: 39

Sun G Y, Liu Q H, Liu Q, Ji C Y and Li X W. 2007. A novel approach for edge detection based on the theory of universal gravity. Pattern Recognition, 40(10): 2766-2775

孙宇彤. 1999. 现代的小卫星技术. 电信快报, (4): 13-15

王晓海. 2002. 蓬勃发展的现代小卫星. 中国航天, (1): 9-14

谢文君, 韦玉春, 倪绍祥, 左伟. 2000. 遥感小卫星的进展. 遥感信息, (3): 41-44

张春雪, 陈秀宏. 2011. 基于非线性滤波的万有引力边缘检测方法. 计算机应用, 31(3): 763-766